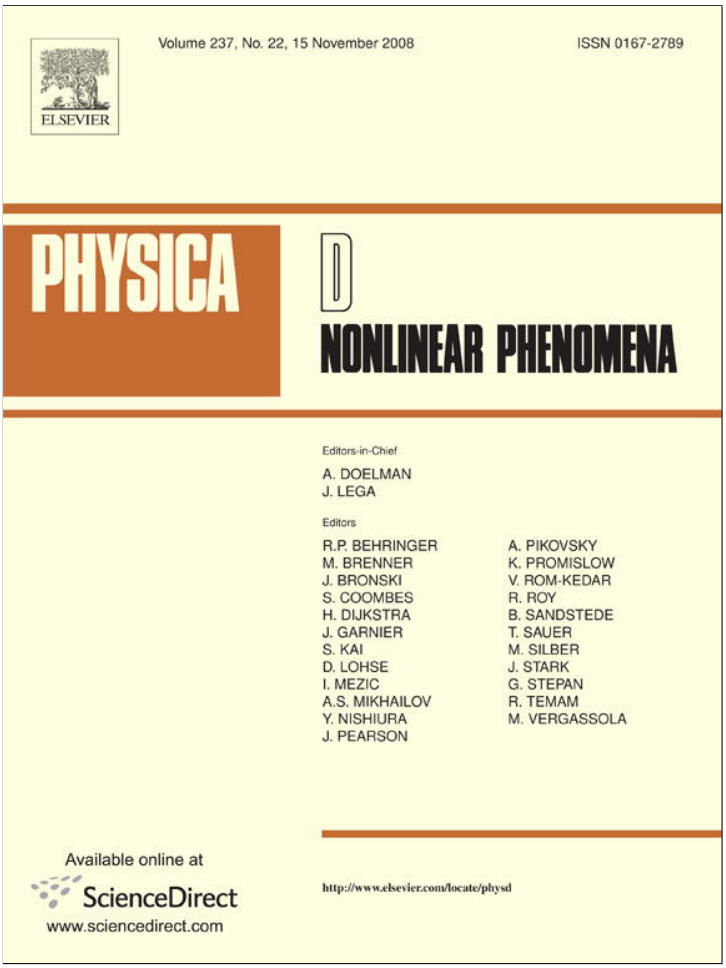

Available online at www.sciencedirect.com
ScienceDirect
Physica D 237 (2008) 2900–2912
PHYSICA D
www.elsevier.com/locate/physd

Boundary intersection crossing bifurcation in the presence of sliding

Alessandro Colombo

DEI, Politecnico di Milano, Via Ponzio, 34/5, Milan, Italy

Received 1 July 2007; received in revised form 28 April 2008; accepted 6 May 2008
Available online 20 May 2008

Communicated by S. Coombes

Abstract

Piecewise smooth systems are known to present a richer set of bifurcations than their smooth counterparts. An interesting family of bifurcations that is present in this type of systems are the so called boundary intersection crossing bifurcations, that take place when a periodic orbit crosses the intersection between two or more discontinuity boundaries. Such bifurcations have been observed in many different models, and have been studied in a number of papers over the past few years. Nonetheless, the particular case in which sliding solutions (as defined by Filippov) are involved, has been left out in previous analyses. This paper addresses this particular case, carrying out a complete analysis and deriving the discontinuity mappings that can be used to characterise such bifurcations. Then, in the second part of the paper, the results are applied to the study of a model of a common electronic device, showing how the mappings can be used systematically to determine the dynamics around the bifurcation.

Keywords: Piecewise smooth; Bifurcation; Discontinuity mapping

1. Introduction

When modelling phenomena from engineering, physical, social and natural sciences, one often has to deal with events that happen on a much shorter time scale than that characterising the main dynamics of the phenomenon. In these cases, a simple and quite common approach consists of recurring to a discontinuous system. In particular, a class of discontinuous systems that has been the subject of much attention in the last few decades is that of piecewise smooth systems, which have been studied by Filippov [1, 2], and more recently have been the subject of a number of publications ([3–5] to cite just a few). An autonomous, continuous-time piecewise smooth system in $\mathbb{R}^n$ is a finite family of ODEs of the form

$$\dot{x} = f^{(i)}(x), \quad x \in S_i \tag{1}$$

where S_i are open non overlapping regions of $\mathbb{R}^n$ separated by $(n-1)$-dimensional manifolds Σ (called *discontinuity boundaries*), such that $\bigcup_i \bar{S}_i$ is the whole state space (the bar indicating the closure of a set). Vector valued functions $f^{(i)}$ are smooth in an open set containing $\bar{S}_i$. In the definition given by Filippov such systems can have, under conditions that are detailed in the next section, orbits that slide along a discontinuity boundary. These orbits are called *sliding solutions*.

It has been observed now in countless examples that the interaction of equilibria and periodic solutions of piecewise smooth systems with the discontinuity boundaries can give place to sudden changes in the dynamics of the system, and to exotic phenomena like period adding cascades and sudden transition to chaos [6–9]. These transitions, that critically involve the presence of one or more discontinuity boundaries, are commonly known as *discontinuity induced bifurcations*. As a consequence, a key to understanding the dynamics of piecewise smooth systems lies in predicting the set of equilibria and periodic solutions that must

E-mail address: alessandro.colombo@polimi.it.

0167-2789/$ - see front matter
doi:10.1016/j.physd.2008.05.002

exist in a neighbourhood of one of such discontinuity induced bifurcations. A first step in this direction was taken by Feigin [10–12], who analysed transitions in piecewise smooth maps. In particular, he considered the behaviour of piecewise smooth linear maps continuous across the discontinuity boundary. In this case, the bifurcations of the simple period-one and -two solutions can be characterised considering the eigenvalues or the characteristic polynomials of the two maps and their iterates. For more recent publications on this subject, the reader can refer to [5,13–15]. The same approach can be applied to periodic orbits in continuous-time piecewise smooth systems, by recurring to Poincaré maps. The dynamical regimes near the bifurcation can then be predicted based on the type of discontinuity of the Poincaré map [5,6,16–19]. Depending on the geometry of the interacton between the orbit and the discontinuity boundary, such Poincaré maps have been shown to be piecewise linear in some cases, so that one can apply directly Feigin's results, or to have quadratic, square root, $3/2$ or other types of discontinuity, in which case further analysis is necessary. In turn, while the Poincaré map depends on the global properties of the system, the discontinuity observed in the map can be derived for general cases by evaluating an appropriate *discontinuity mapping*, which is a local mapping defined as the "correction" that must be applied to the system trajectories in order to account for the presence of the discontinuity boundary. This approach, which is the one we follow in this paper, allows one to set aside the specific details of the studied system, and to obtain general results that depend only on the local geometry of vector fields near the discontinuity boundaries.

We study a class of discontinuity induced bifurcations that is caused by the interaction between periodic orbits and the intersection of two or more discontinuity boundaries or, equivalently, between periodic orbits and corners of the discontinuity boundaries. These bifurcations are quite common in mechanical and electrical systems with more than one source of discontinuity (and thus more than one boundary) or with nonsmooth discontinuity boundaries (i.e. boundaries composed of smooth surfaces pieced together at corners). Bifurcations involving the intersection of boundaries have been called *boundary intersection crossings* [5,20], while bifurcations involving corners are referred to as *corner collisions* [16]. For these bifurcations, a general analysis is extremely difficult, due to the great number of qualitatively different configurations, so that up to now only a very limited number of instances have been analysed, motivated by specific applications. In particular, in [16] the authors analysed particular cases of corner collision, whereas a more general instance of the problem was studied in [5], where the case of two intersecting discontinuity boundaries and four vector fields (with strong constraints on the geometry of the vector fields) was analysed. In all the examples analysed in the literature, the possibility of having sliding solutions in a neighbourhood of the boundary intersection have been excluded, even though sliding phenomena are common in piecewise smooth systems like dry friction models [21], power converters [22] or variable structure control models [23]. Therefore, it is worth extending the work done so far to include cases where sliding occurs in the neighbourhood of the boundary intersection. In what follows, we derive for the first time, the discontinuity mapping for these types of bifurcation, in the case of two intersecting boundaries, in a setting that is as general as possible without becoming overly complicated. In particular, the next section is devoted to some observations on uniqueness of solutions in the presence of boundary intersections. Then, in Section 3 we explain in more detail the concept of zero-time discontinuity mapping (ZDM) and of Poincaré discontinuity mapping (PDM) and derive the maps analytically. In Section 4 we apply the results to the analysis of a model of buck converter. Finally, in Section 5 we draw some conclusions.

2. Uniqueness of solutions at the intersection of discontinuity boundaries

Before proceeding, it is worth making some observations on the uniqueness of solutions at the intersection of discontinuity boundaries. We define solutions on discontinuity boundaries using Filippov convex method, which we report here briefly (for more details, see [1,2,24]).

Consider the system described in (1), and define for each point x, a set $F(x)$. If the point x belongs to the interior of a region S_i then the set $F(x)$ consists of one point and coincides with the value of $f^{(i)}(x)$. On the other hand, if x belongs to the boundary between two or more regions $S_i, S_j, \ldots$, then $F(x)$ is the smallest closed convex set containing the limit values of $f^{(i)}(x^*)$, $f^{(j)}(x^*), \ldots$, for $x^* \to x$. We can now define solutions of system (1) as solutions of the differential inclusion

$$\dot{x} \in F(x). \tag{2}$$

A segment of solution is called a *standard solution* if it is a solution of one of the vector fields $f^{(i)}(x)$, $x \in S_i$, while it is called a *sliding solution* if it is a solution of a *sliding vector field* $f^{(s)}$, convex combination of two or more vector fields $f^{(i)}$ along one or more discontinuity boundaries (see Fig. 1). Notice that, in the simple case of a single discontinuity boundary separating two regions, a sliding solution exists only if the components of the two vector fields normal to the boundary point in opposite directions. In this case, the region where sliding solutions exist is called a stable sliding region if the two vector fields point toward the boundary, and is called unstable sliding region otherwise.

As one can see, solutions of an initial value problem are not necessarily unique. In particular, at a boundary intersection there are two cases that can give rise to non-uniqueness of solutions. First, two or more inflowing vector fields (which are, roughly speaking, vector fields pointing inward in their respective regions of definition) can be defined at the boundary intersection. In this case there are as many solutions as there are inflowing vector fields. Second, the subset of $F(x)$ tangent to the boundary intersection manifold may contain more than one vector, in which case there are many (infinite) different sliding solutions along the boundary intersection manifold. In both cases, the choice of solution depends on the particular phenomenon being modeled, and the problem cannot be

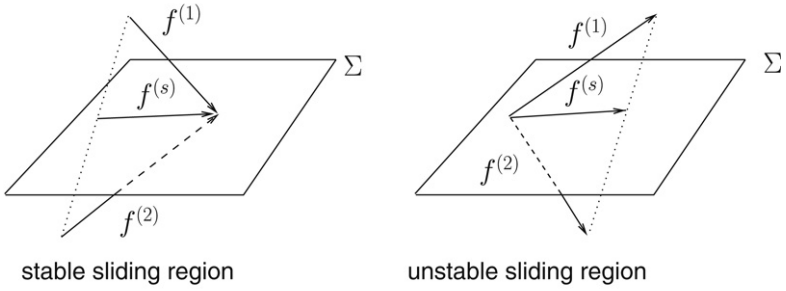

Fig. 1. A sliding region is said to be stable when the vector fields $f^{(1)}$ and $f^{(2)}$ on both sides of the discontinuity boundary Σ point toward the boundary, while it is unstable if the vector fields $f^{(1)}$ and $f^{(2)}$ point away from the boundary. The sliding vector field $f^{(s)}$ is the convex combination of $f^{(1)}$ and $f^{(2)}$ tangent to Σ.

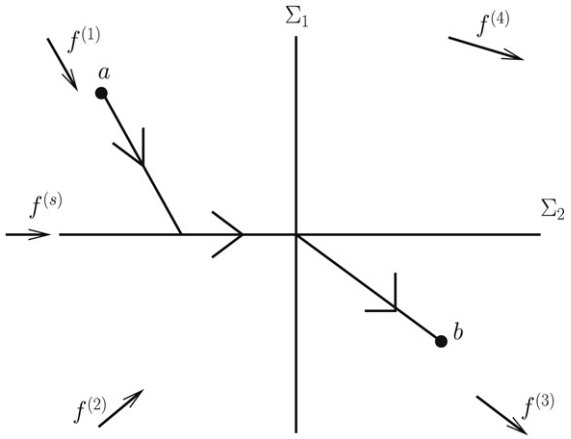

Fig. 2. An orbit in a planar system with two discontinuity boundaries and four different vector fields.

treated in a general way. Therefore, in the rest of the paper, we carefully exclude those cases that can give rise to non-unique solutions.

3. Discontinuity mapping

We proceed now to defining and deriving the discontinuity mappings in a neighbourhood of the intersection of two discontinuity boundaries. In the rest of this paper, the discontinuity boundaries are called Σ_1 and Σ_2. We perform a local analysis around a point p, located at the intersection between Σ_1 and Σ_2, and suppose that the two boundaries intersect transversally. In a neighbourhood of p the discontinuity boundaries are described by the zero sets of two smooth functions $H_1(x)$ and $H_2(x)$ with non-vanishing gradient (thus, Σ_1 and Σ_2 are locally smooth manifolds). The state space around p is divided by the boundaries into four regions $S_1 \ldots S_4$, corresponding to four vector fields $f^{(1)} \ldots f^{(4)}$ (see for example Fig. 2). Finally, orbits across the boundaries and sliding orbits on the boundaries are defined using Filippov convex method, as explained in the previous section.

3.1. The concept of discontinuity mapping

As we said in the introduction, a discontinuity mapping is a map defining the correction that must be applied to the orbits of a system in order to account for the presence of a discontinuity boundary. Considering for example the bi-dimensional case depicted in Fig. 2, call $\Phi_i(x, t)$ the flow of x generated by vector field $f^{(i)}$. We want to write point b as

$$b = \Phi_3(DM(\Phi_1(a, t_1)), t_2), \tag{3}$$

where DM is the discontinuity mapping. In the literature two different forms of discontinuity mapping have been proposed, useful in different situations: the *Poincaré discontinuity mapping* (PDM) and the *zero-time discontinuity mapping* (ZDM). To understand how these mappings are obtained, consider the orbit from a to b in Fig. 3. In order to derive the PDM (Fig. 3a), we must choose a suitable Poincaré section, which we conveniently place on the discontinuity boundary Σ_1. Then, t_1 is the time necessary to the trajectory $\Phi_1(a, t)$ to reach the Poincaré section, and the DM is the mapping that must be applied to the points on this section in order for Eq. (3) to be correct. Calling x_0 the point where the trajectory intersects the Poincaré section, we can write the PDM as

$$\text{PDM} = \Phi_s(\Phi_1(x_0, \tau_1), \tau_2).$$

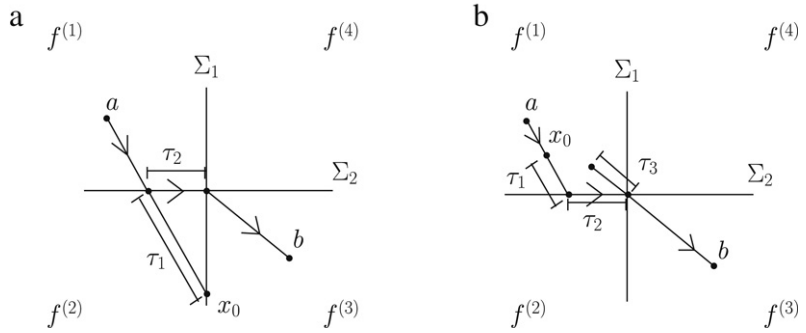

Fig. 3. Two ways of constructing a discontinuity mapping for the case depicted in Fig. 2. In (a), the PDM is found by integrating backward from x_0 on Σ_1 for a time τ_1 along the vector field $f^{(1)}$, and then forward for a time τ_2 along the vector field $f^{(s)}$. In (b), the ZDM is constructed by integrating from a point x_0 on $\phi(a, t)$ for a time τ_1 along the vector field $f^{(1)}$, then for a time τ_2 along the vector field $f^{(s)}$ and finally for a time τ_3 along the vector field $f^{(3)}$, where $\tau_1 + \tau_2 + \tau_3 = 0$.

Notice that τ_1 must be negative.

In the case of the ZDM (Fig. 3b), t_1 is the time necessary for the aforementioned trajectory to come close (in some norm) to the boundary intersection. Then, the DM is the mapping to be applied to $x_0 = \Phi_1(a, t_1)$ so that Eq. (3) is correct and so that the total time $t_1 + t_2$ in (3) is equal to the time necessary to go from a to b in the real system, taking into account all the discontinuity boundaries. In other words, in this case the mapping must preserve time. Notice that now x_0 is not bound to lie on Σ_1. Referring to Fig. 3b we have

$$\text{ZDM} = \Phi_3(\Phi_s(\Phi_1(x_0, \tau_1), \tau_2), \tau_3),$$

with the additional constraint that $\tau_1 + \tau_2 + \tau_3 = 0$. Notice that, as expected, both the PDM and the ZDM have different functional forms for orbits intersecting first Σ_1 and then Σ_2 or vice versa.

3.2. Derivation of the discontinuity mappings

We now proceed with the derivation of the ZDM and PDM in an n-dimensional system, around a point p located at the intersection of two discontinuity boundaries in the presence of sliding.

There are in principle 256 ways of arranging the vector fields around a boundary intersection, because on each one of the four half boundaries solutions can slide towards or away from the intersection, or can cross the boundary clockwise or counterclockwise, and this without counting the possibility of sliding along the intersection. Of these cases, 240 have at least one sliding region in the neighbourhood of the boundary intersection. Even if we cancel the cases that are topologically equivalent, through reflection and rotation, and those that involve non uniqueness of solutions, the number of possible configurations remains large. In order to keep the problem simple and to make the presentation readable, we assume that there is only one stable sliding region (and no unstable one) near the intersection, for example in the region between S_1 and S_2, and that the sliding vector field points toward the boundary intersection. The mapping for all other cases, though generally different, can be obtained with similar calculations. Supposing to have $H_1(x) > 0$ and $H_2(x) > 0$ for $x \in S_1$ (any other choice would just change the direction of the inequalities), these assumptions can be expressed by the following conditions, valid in a neighbourhood of p:

$$\mathcal{L}_{f^{(1)}} H_1(x) \mathcal{L}_{f^{(4)}} H_1(x) > 0, \tag{4}$$

$$\mathcal{L}_{f^{(2)}} H_1(x) \mathcal{L}_{f^{(3)}} H_1(x) > 0, \tag{5}$$

$$\mathcal{L}_{f^{(4)}} H_2(x) \mathcal{L}_{f^{(3)}} H_2(x) > 0, \tag{6}$$

$$\mathcal{L}_{f^{(1)}} H_2(x) \mathcal{L}_{f^{(2)}} H_2(x) < 0, \tag{7}$$

$$\mathcal{L}_{f^{(1)}} H_2(x) < 0, \tag{8}$$

$$\mathcal{L}_{f^{(1)}} H_1(x) < 0, \tag{9}$$

$$\mathcal{L}_{f^{(2)}} H_1(x) < 0, \tag{10}$$

where $\mathcal{L}_{f^{(i)}} H_j(x)$ is the Lie derivative of $H_j(x)$ with respect to $f^{(i)}(x)$, that is, the derivative of the function $H_j(x)$ along the vector field $f^{(i)}(x)$. Conditions (4)–(7) make sure that there is only one sliding region, condition (8) insure that the sliding region is stable, and conditions (9) and (10) make sure that sliding trajectories approach the boundary intersection manifold. Moreover, in order to exclude pathological cases, we assume that $f^{(1)} \dots f^{(4)}$ are non vanishing. Notice that under these conditions there is one and only one inflowing vector field at each point of the boundary intersection manifold, and conditions (4), (5), (9) and (10) together insure that the set $F(x)$ in Eq. (2) has no component along the boundary intersection manifold. Therefore, solutions starting on

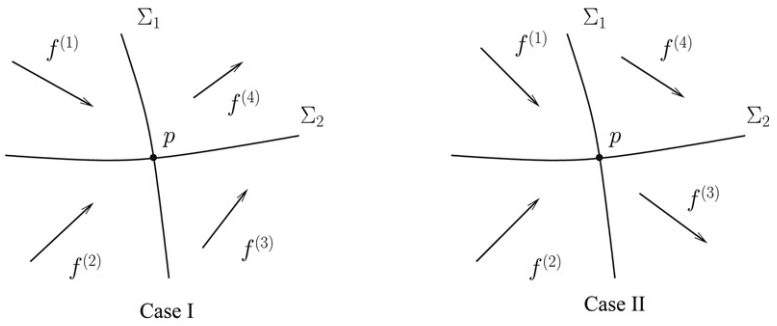

Fig. 4. Sketch of the geometry of the state space in case I and case II.

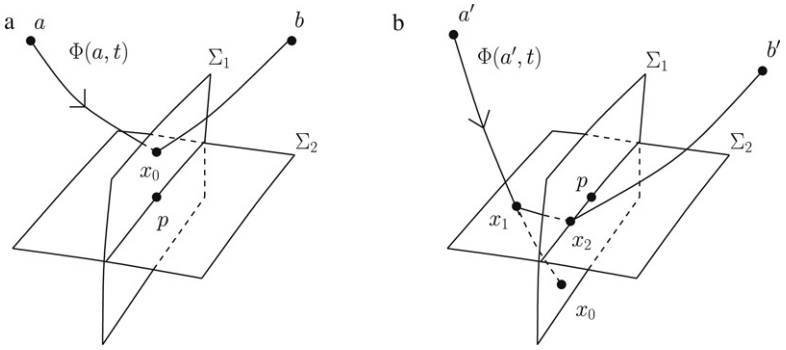

Fig. 5. Construction of the PDM in case I, see text for details.

the boundary intersection manifold are unique in forward time. In order to proceed with the analysis we suppose that the trajectory starts from a point a in S_1, and we distinguish between the two following cases (as depicted in Fig. 4):

I $\mathcal{L}_{f^{(4)}} H_2(x) > 0$,
II $\mathcal{L}_{f^{(4)}} H_2(x) < 0$.

Notice that the vector fields in the two cases are indeed equivalent under reflection through Σ_2, and we could as well consider just one configuration, with point a being in S_1 for case I and in S_2 for case II.

The subsequent analysis is carried out in the general n-dimensional case.

Case I

Derivation of the PDM

We start by deriving the PDM for case I. As explained previously, we place the Poincaré section on the discontinuity boundary Σ_1. Conditions (4) and (5) ensure that all orbits cross this section transversally. In Fig. 5 two orbits are represented crossing the Poincaré section in a neighbourhood of p: $\Phi(a,t)$, that crosses the Poincaré section without intersecting the sliding region on Σ_2, and $\Phi(a',t)$, that intersects the sliding region. Clearly, no correction must be applied to orbit $\Phi(a,t)$ (and to any orbit such that $H_2(x_0) > 0$), for which the PDM is the identity. In the case of orbit $\Phi(a',t)$ (and any orbit such that $H_2(x_0) < 0$) instead we must find the map from x_0 to x_2, as shown in Fig. 5b. This requires integrating the vector field $f^{(1)}$ backward in time from x_0 to x_1, and then integrating the sliding vector field $f^{(s)}$ forward in time from x_1 to x_2.

We have

$$\begin{aligned} &x_2 = \Phi_s(\Phi_1(x_0,\tau_1),\tau_2),\\ &H_2(x_1) = H_2(\Phi_1(x_0,\tau_1)) = 0,\\ &H_1(x_2) = H_1(\Phi_s(\Phi_1(x_0,\tau_1)),\tau_2) = 0. \end{aligned}$$

If x_0 is sufficiently close to p, meaning that $\|x_0 - p\| \ll 1$, we can suppose that both τ_1 and τ_2 are short, and do a first order expansion around $\tau_1 = \tau_2 = 0$ of the previous equations, giving

$$x_2 = x_0 + f^{(1)}(x_0)\tau_1 + f^{(s)}(x_0)\tau_2 + O(2), \tag{11}$$

$$H_2(x_0) + \mathcal{L}_{f^{(1)}} H_2(x_0)\tau_1 + O(2) = 0, \tag{12}$$

$$H_1(x_0) + \mathcal{L}_{f^{(1)}} H_1(x_0)\tau_1 + \mathcal{L}_{f^{(s)}} H_1(x_0)\tau_2 + O(2) = 0, \tag{13}$$

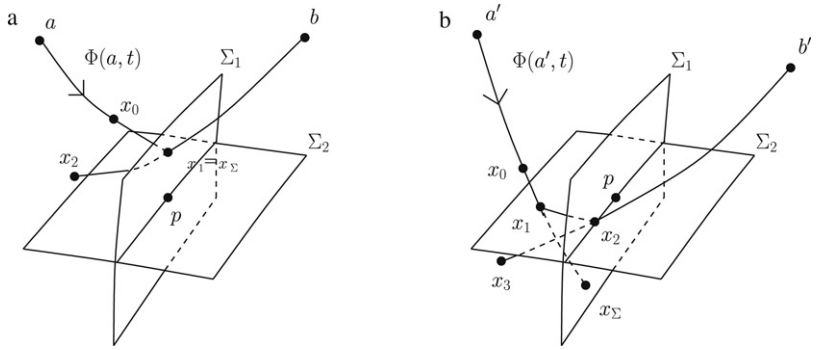

Fig. 6. Construction of the ZDM in case I, see text for details.

where $O(2)$ are quadratic terms in τ_1 and τ_2 and cross products $\tau_1\tau_2$. Notice that $H_1(x_0) = 0$. Conditions (8)–(10) allow us to solve (12) and (13) for τ_1 and τ_2. Then substituting τ_1 and τ_2 in (11) and getting rid of the higher order terms we obtain the first order expansion of the mapping

$$x_2 = \begin{cases} x_0, & H_2(x_0) \geq 0, \\ x_0 - f^{(1)}\left(\dfrac{H_2}{\mathcal{L}_{f^{(1)}}H_2}\right) + f^{(s)}\left(\dfrac{\mathcal{L}_{f^{(1)}}H_1}{\mathcal{L}_{f^{(s)}}H_1}\dfrac{H_2}{\mathcal{L}_{f^{(1)}}H_2}\right), & H_2(x_0) < 0. \end{cases}$$

Here, for sake of clarity, we have omitted to write the dependence of H_i and $f^{(i)}$ on x, keeping in mind that all quantities must be evaluated at x_0. As one can see, this mapping is continuous across the surface $H_2(x) = 0$. We can linearise the mapping around p, substituting $\delta x = x_0 - p$, and obtain the following piecewise linear continuous mapping

$$\delta x_2 = \begin{cases} \delta x_0, & H_2(x_0) \geq 0, \\ \left(I - \dfrac{(H_{1x}^T f^{(s)})f^{(1)}H_{2x}^T - (H_{1x}^T f^{(1)})f^{(s)}H_{2x}^T}{H_{1x}^T f^{(s)} H_{2x}^T f^{(1)}}\right)\delta x_0, & H_2(x_0) < 0, \end{cases} \tag{14}$$

where H_{ix} is the gradient of H_i, and all H_i and $f^{(i)}$ are evaluated at p. Notice that the above Jacobian is singular in the case $H_2(x_0) < 0$, with the null vector

$$f^{(1)} - f^{(s)}\frac{H_{1x}^T f^{(1)}}{H_{1x}^T f^{(s)}}.$$

This is a general consequence of the presence of a sliding region (and it is true in all following mappings), as sliding solutions are not unique backward in time. Thus, we have shown that the local expression for this discontinuity mapping is piecewise linear and dimension reducing in presence of sliding. Note that Kowalczyk [25] (see also [5]), analysed the dynamics of such maps, showing that they can undergo transitions to robust chaotic attractors that (in two dimensions) lie on segments.

Derivation of the ZDM

With similar algebra, we can derive the ZDM for case I. In this case, as noticed before, x_0 does not have to lie on Σ_1. Therefore, in order to distinguish between trajectories crossing Σ_1 above or below Σ_2, we consider the point x_Σ located at the first intersection of the trajectory with Σ_1, as shown in Fig. 6. In this case the mapping is (see the Appendix for details)

$$x_3 = \begin{cases} x_0 + (f^{(4)} - f^{(1)})\left(\dfrac{H_1}{\mathcal{L}_{f^{(1)}}H_1}\right), & H_2(x_\Sigma) > 0, \\ x_0 + (f^{(4)} - f^{(1)})\left(\dfrac{H_2}{\mathcal{L}_{f^{(1)}}H_2}\right) + (f^{(s)} - f^{(4)})\left(\dfrac{H_2\mathcal{L}_{f^{(1)}}H_1 - H_1\mathcal{L}_{f^{(1)}}H_2}{\mathcal{L}_{f^{(s)}}H_1\mathcal{L}_{f^{(1)}}H_2}\right), & H_2(x_\Sigma) < 0. \end{cases}$$

Once again, linearising about p we obtain

$$\delta x_3 = \begin{cases} \left(I + (f^{(4)} - f^{(1)})\left(\dfrac{H_{1x}^T}{H_{1x}^T f^{(1)}}\right)\right)\delta x_0, & H_2(x_\Sigma) > 0, \\ \left(I + (f^{(4)} - f^{(1)})\left(\dfrac{H_{2x}^T}{H_{2x}^T f^{(1)}}\right) + (f^{(s)} - f^{(4)})\left(\dfrac{(H_{1x}^T f^{(1)})H_{2x}^T - (H_{2x}^T f^{(1)})H_{1x}^T}{H_{1x}^T f^{(s)} H_{2x}^T f^{(1)}}\right)\right)\delta x_0, & H_2(x_\Sigma) < 0. \end{cases}$$

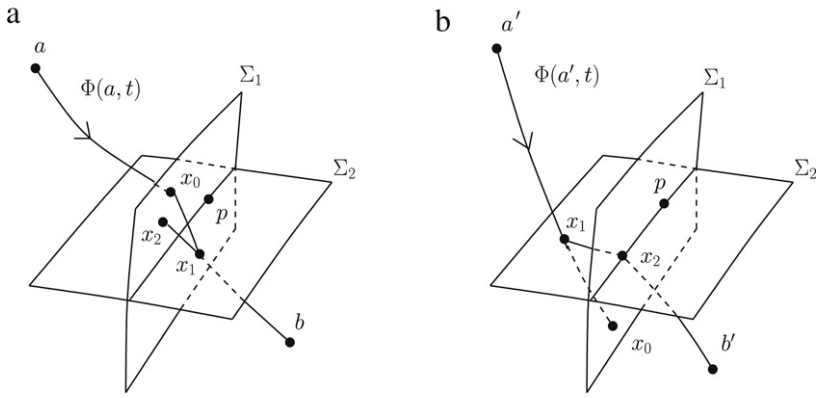

Fig. 7. Construction of the PDM in case II, see text for details.

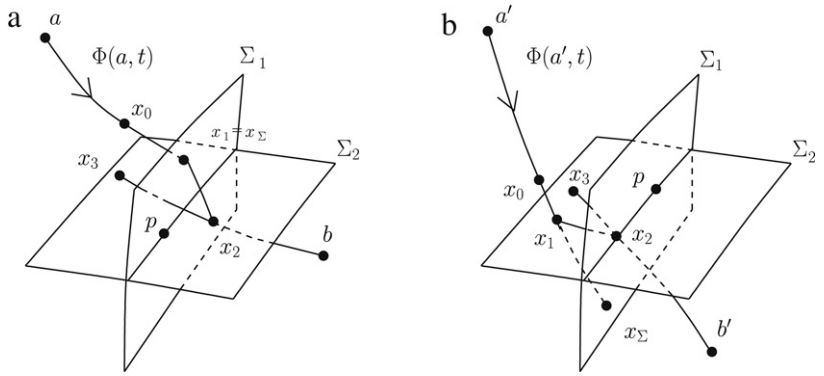

Fig. 8. Construction of the ZDM in case II, see text for details.

Case II.

In this case, the mappings for $H_2(x_0) < 0$ and $H_2(x_\Sigma) < 0$ have the same form of those presented before, with the only difference that in the ZDM vector field $f^{(4)}$ must be substituted with vector field $f^{(3)}$ at every appearance. On the other hand, the mappings for $H_2(x_0) > 0$ and $H_2(x_\Sigma) > 0$ are now different due to the different sequence of events for such trajectories. The steps are, once again, similar to those used for the derivation of the PDM in case I, and we relegate the details to the Appendix.

Derivation of the PDM

The PDM for case II, represented in Fig. 7, is

$$x_2 = \begin{cases} x_0 - f^{(4)} \dfrac{H_2}{\mathcal{L}_{f^{(4)}} H_2} - f^{(3)} \dfrac{\mathcal{L}_{f^{(4)}} H_1}{\mathcal{L}_{f^{(s)}} H_1} \dfrac{H_2}{\mathcal{L}_{f^{(4)}} H_2}, & H_2(x_0) > 0, \\ x_0 - f^{(1)} \left(\dfrac{H_2}{\mathcal{L}_{f^{(1)}} H_2} \right) + f^{(s)} \left(\dfrac{\mathcal{L}_{f^{(1)}} H_1}{\mathcal{L}_{f^{(s)}} H_1} \dfrac{H_2}{\mathcal{L}_{f^{(1)}} H_2} \right), & H_2(x_0) < 0, \end{cases}$$

which can be linearised to obtain

$$\delta x_2 = \begin{cases} \left(I - f^{(4)} \dfrac{H_{2x}^T}{H_{2x}^T f^{(4)}} - f^{(3)} \dfrac{H_{1x}^T f^{(4)}}{H_{1x}^T f^{(s)}} \dfrac{H_{2x}^T}{H_{2x}^T f^{(4)}} \right) \delta x_0, & H_2(x_0) > 0, \\ \left(I - f^{(1)} \left(\dfrac{H_{2x}^T}{H_{2x}^T f^{(1)}} \right) + f^{(s)} \left(\dfrac{H_{1x}^T f^{(1)}}{H_{1x}^T f^{(s)}} \dfrac{H_{2x}^T}{H_{2x}^T f^{(1)}} \right) \right) \delta x_0, & H_2(x_0) < 0. \end{cases}$$

Derivation of the ZDM

The ZDM (Fig. 8), is instead

$$x_3 = \begin{cases} x_0 + (f^{(4)} - f^{(1)}) \dfrac{H_2}{\mathcal{L}_{f^{(1)}} H_2}, & H_2(x_\Sigma) > 0, \\ x_0 + (f^{(3)} - f^{(1)}) \left(\dfrac{H_2}{\mathcal{L}_{f^{(1)}} H_2} \right) + (f^{(s)} - f^{(3)}) \left(\dfrac{H_2 \mathcal{L}_{f^{(1)}} H_1 - H_1 \mathcal{L}_{f^{(1)}} H_2}{\mathcal{L}_{f^{(s)}} H_1 \mathcal{L}_{f^{(1)}} H_2} \right), & H_2(x_\Sigma) < 0, \end{cases}$$

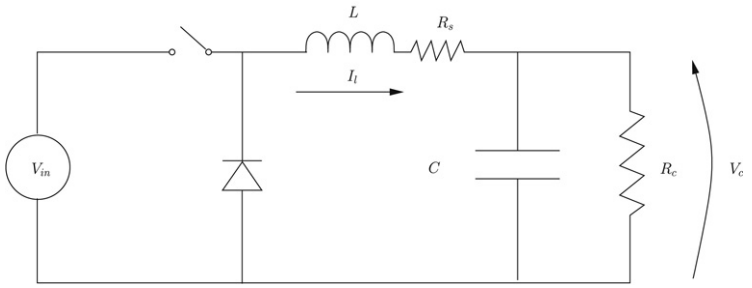

Fig. 9. Schematic diagram of the buck converter.

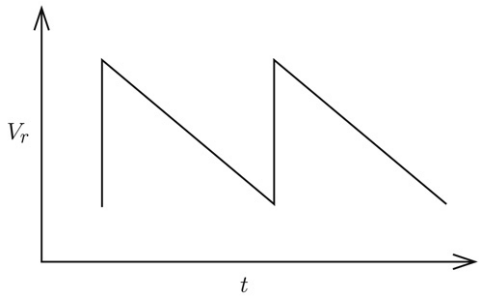

Fig. 10. The sawtooth reference voltage signal V_r.

which can be linearised to obtain

$$\delta x_3 = \begin{cases} \left(I + (f^{(4)} - f^{(1)}) \dfrac{H_{2x}^T}{H_{2x}^T f^{(1)}} \right) \delta x_0, & H_2(x_\Sigma) > 0, \\ \left(I + (f^{(3)} - f^{(1)}) \left(\dfrac{H_{2x}^T}{H_{2x}^T f^{(1)}} \right) + (f^{(s)} - f^{(3)}) \left(\dfrac{H_{1x}^T f^{(1)} H_{2x}^T - H_{2x}^T f^{(1)} H_{1x}^T}{H_{1x}^T f^{(s)} H_{2x}^T f^{(1)}} \right) \right) \delta x_0, & H_2(x_\Sigma) < 0. \end{cases}$$

This completes the set of discontinuity mappings for the case under study.

4. Application to a Buck converter

Here we apply the results obtained in the previous section to the analysis of a boundary intersection crossing bifurcation in a model of the buck converter, a type of DC/DC step-down conversion circuit. This is a common component of modern commercial electronics, such as power supplies for laptop computers and similar products, owing to its high energy efficiency. Nonsmooth bifurcations have already been treated in the past for this type of circuit, both through extensive numerical exploration of the parameter space [26,27] and with analytical methods [16,22]. However, no analytical approach to boundary intersections in presence of sliding have been undertaken so far.

The basic circuit is shown in Fig. 9. In the most popular implementation, called pulse width modulation (PWM), the duty cycle of the switch is controlled by some external logic, and in general the switch is opened or closed based on the comparison between the output voltage V_c and a periodic signal V_r of period T. In this paper, in accordance with a number of previous studies, we suppose that V_r is an inverse sawtooth, as represented in Fig. 10. The average value of the sawtooth signal is V_{av} and its peak to peak amplitude is V_{amp}. Overall the circuit can be described by the following equations:

$$\dot{V}_c = -\frac{V_c}{R_c C} + \frac{I_l}{C},$$

$$\dot{I}_l = \begin{cases} -\dfrac{V_c}{L} - \dfrac{R_s I_l}{L}, & V_c > V_r, I_l > 0, \\ 0, & V_c > V_r, I_l = 0, \\ -\dfrac{V_c}{L} - \dfrac{R_s I_l}{L} + \dfrac{V_{in}}{L}, & V_c < V_r. \end{cases}$$

Here L and R_s are the inductance and its equivalent series resistance, C is the capacitance, R_c is the load resistance and V_{in} is the input voltage. The circuit thus operates in three different topologies, corresponding to three vector fields (see Fig. 13 for a sketch of the state space):

$f^{(1)}$ when $V_c > V_r, I_l > 0$,

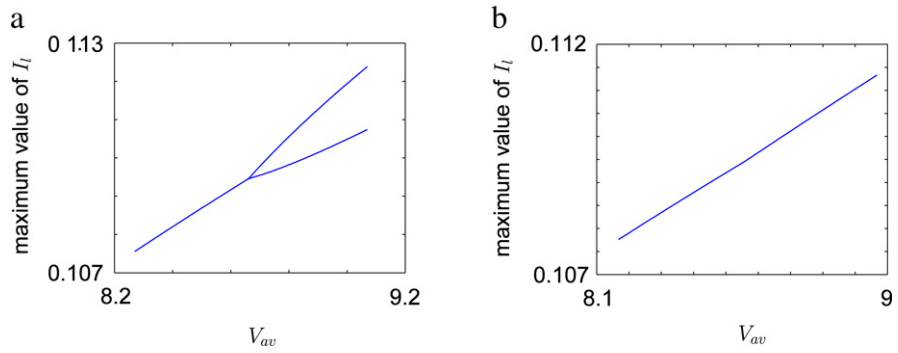

Fig. 11. Bifurcation plots in V_{av} of the buck converter for two sets of parameters. In (a), $V_{amp} = 5.6$ and the bifurcation takes place at $V_{av} = 8.67$. In (b), $V_{amp} = 8$ and the bifurcation takes place at $V_{av} = 8.568$. The other parameters are the same for the two examples and have the following values: $R_s = 4.35$, $R_c = 163$, $T = 4.234e-4$, $V_{in} = 20$, $L = 20e-3$, $C = 4.7e-6$.

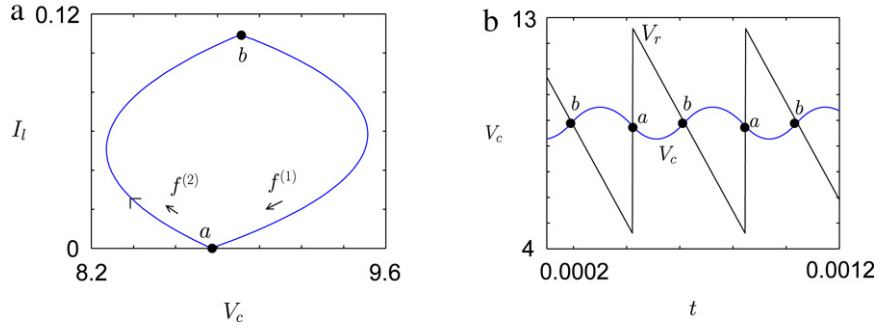

Fig. 12. The bifurcating orbit (a) in the (V_c, I_l) plane and (b) in the (t, V_c) plane. In (b) the sawtooth signal V_r is also represented. Notice that the orbit crosses the boundary intersection at point a.

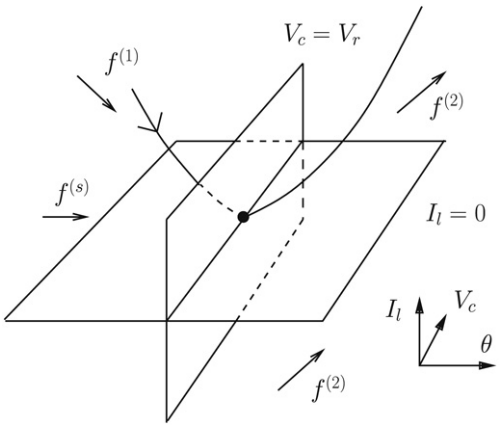

Fig. 13. Sketch of the orbit depicted in Fig. 11 nar the boundary intersection.

$f^{(s)}$ when $V_c > V_r$, $I_l = 0$,
$f^{(2)}$ when $V_c < V_r$.

First of all, in order to make the system autonomous, we must extend the state (V_c, I_l) to include the phase of the T-periodic sawtooth signal. We therefore deal with a three dimensional cylindrical state space with state $(V_c, I_l, \theta) \in \mathbb{R}^2 \times \mathbb{R}/\mathbb{Z}T$. Notice that the behaviour of the circuit in this model is not defined when $V_c > V_r$ and $I_l < 0$. Nevertheless, this region of the state space is not reachable from its complementary region, therefore we are free to choose any vector field as long as it is consistent with the sliding vector field $f^{(s)}$ on the boundary $I_l = 0$.

We can now move on to the analysis of a bifurcation involving the intersection between the boundaries $I_l = 0$ and $V_c = V_r$. Consider the system corresponding to Fig. 11a, in which we have plotted the local maxima along the I_l axis of a periodic attractor. At the critical value $V_{av} = 8.67$ the attractor undergoes a boundary intersection crossing bifurcation that causes a period doubling, as one can see in the figure. The orbit at the bifurcation point is plotted in Fig. 12, while Fig. 13 sketches the geometry of the

state space in a neighbourhood of the boundary intersection crossing point. Notice that a similar bifurcation is found for periodic orbits hitting a corner of the sawtooth signal, if a combination of V_c and I_l is used as triggering value to compare with V_r. As one can see, the configuration of the vector fields corresponds to case I treated in the previous section. We know that the discontinuity mapping for a periodic orbit passing through this intersection is piecewise linear to leading order, therefore we can characterise the bifurcation using Feigin's approach by checking the eigenvalues of the linearised Poincaré map in a neighbourhood of the bifurcating orbit. The reader can refer to the abundant literature on the subject [5,6,16,17,19,28] for details on this matter, while here we simply report the few details needed in this particular case. Consider the two sets of eigenvalues of the map immediately before and after the bifurcation. We expect the periodic orbit to exist on both sides of the bifurcation if the total number of real eigenvalues bigger than 1 is even, while the orbit exists only on one side if this number is odd. At the same time, we expect a solution with double period to originate at the bifurcation if the total number of real eigenvalues smaller than -1 is odd.

In order to find the linearised Poincaré map, we choose to use the linearised PDM (14), placing the Poincaré section on the discontinuity boundary $V_c = V_r$. The eigenvalues of the linearised Poincaré map, equal to the non-trivial Floquet multipliers of the cycle (from here on just called "multipliers"), can be found by evaluating the monodromy matrix of the cycle, given by the product

$$M = PDM \cdot M_2 \cdot S \cdot M_1,$$

where M_1 and M_2 are the principal fundamental solution matrices along segments $[a, b]$ and $[b, a]$ in Fig. 12, PDM is the linearised Poincaré discontinuity mapping (14), and S is the saltation matrix giving the necessary correction at point b, which was first described in [29]. Its analytical form is

$$S = I + (f^{(2)} - f^{(1)}) \frac{H_{1x}^T}{H_{1x}^T f^{(1)}}.$$

By numerically evaluating M for the bifurcating cycle, we find that the multipliers are

$$-1.1147 \quad \text{and} \quad -0.4705$$

for an orbit not intersecting the boundary $I_l = 0$, and

$$-0.8962 \quad \text{and} \quad 0$$

for an orbit that intersects the boundary $I_l = 0$. Notice that in the second case one multiplier is equal to zero, due to the non invertibility of the map. The total number of multipliers smaller than -1 being odd, we can correctly conclude that at the bifurcation a solution of double period is born (see Fig. 11a). Moreover, as the total number of real multipliers bigger than 1 is even (always 0), the "period one" solution must exist on both sides of the bifurcation (and we see from the multipliers that it is unstable on one side). A similar analysis for the twice iterated map would finally allow us to conclude that the double period solution exists for $V_{av} > 8.67$. Much in the same way, we can evaluate the multipliers of the bifurcating orbit in the example corresponding to Fig. 11b. In this case the multipliers are

$$-0.6179 + 0.3777\text{i} \quad \text{and} \quad -0.6179 - 0.3777\text{i}$$

for an orbit not intersecting the boundary $I_l = 0$, and

$$-0.7246 \quad \text{and} \quad 0$$

for an orbit that intersects the boundary $I_l = 0$. This time, the total number of real multipliers smaller than -1 is zero, therefore we expect no period doubling, as confirmed by the plot in Fig. 11b.

By repeating this analysis along a bifurcation line we could detect, when one real multiplier crosses the unit circle, points of higher codimension where the bifurcation changes characteristics. These are branching points of the bifurcation diagram, and certainly deserve further attention as they allow us to understand the complex interplay of the different bifurcations that can appear in a discontinuous system. Some studies on these codimension 2 points have been carried out in [20], and a more detailed analysis for the example of the buck converter will be included in a future paper.

5. Conclusions

In the first part of this paper we derived the discontinuity mappings for a boundary intersection crossing bifurcation in the presence of sliding. This extends the analysis done in the past to piecewise smooth systems with sliding, thus filling a gap in the theory of discontinuity induced bifurcations. In the analysis we made a few restrictive assumptions, that do not undermine the applicability of the results. However, the analysis presented does not exhaust the set of possibly interesting scenarios, like cases where more than one sliding segment is present in a neighbourhood of the boundary intersection, and a more general approach is currently under development. Moreover, in this paper we did not attempt to analyse the behaviour of this bifurcation in combination

with other smooth or nonsmooth bifurcations. A correct understanding of the unfolding of these higher codimension cases would be a useful tool in the analysis of discontinuous systems.

In the second part, we presented an example application of the theoretical results to the analysis of bifurcations of a buck converter, which is a common electronic circuit. The example aimed mainly to clarify how the newly derived mapping can be used. Nevertheless, as pointed out in the paper, this approach can be easily implemented in bifurcation analysis software, allowing one to systematically characterise discontinuity induced bifurcations, and to detect bifurcations of higher codimension, thus constituting a key tool for the analysis of bifurcations in discontinuous systems.

Acknowledgements

The author would like to thank Alan Champneys for his useful comments on an early revision of this manuscript. He also acknowledges the Centre de Recerca Matemática, Bellaterra, Spain, for hospitality during the preparation of the manuscript. Financial support was partially provided by MIUR under project PRIN2005-098133.

Appendix

In the following paragraphs we report the details of the derivation of the discontinuity mapping that have been left out in the text. In the discontinuity mappings reported here, we omit the explicit dependence of $f^{(i)}$ and H_i on x, keeping in mind that all quantities must be evalueated at x_0.

A.1. Case I, ZDM, $H_2(x_\Sigma) > 0$

We have,

$$\begin{aligned}
&x_2 = \Phi_4(\Phi_1(x_0, \tau_1), \tau_2),\\
&H_1(x_1) = H_1(\Phi_1(x_0, \tau_1)) = 0,\\
&\tau_1 + \tau_2 = 0.
\end{aligned}$$

Expanding about $\tau_1 = 0$, we obtain

$$\begin{aligned}
&x_2 = x_0 + f^{(1)}(x_0)\tau_1 + f^{(4)}(x_0)\tau_2 + O(2),\\
&H_1(x_0) + \mathcal{L}_{f^{(1)}} H_1(x_0)\tau_1 = 0,\\
&\tau_1 = -\tau_2.
\end{aligned}$$

Hence,

$$x_2 = x_0 + (f^{(4)} - f^{(1)})\frac{H_1}{\mathcal{L}_{f^{(1)}} H_1}$$

A.2. Case I, ZDM, $H_2(x_\Sigma) < 0$

We have,

$$\begin{aligned}
&x_3 = \Phi_4(\Phi_s(\Phi_1(x_0, \tau_1), \tau_2), \tau_3),\\
&H_2(x_1) = H_2(\Phi_1(x_0, \tau_1)) = 0,\\
&H_1(x_2) = H_1(\Phi_s(\Phi_1(x_0, \tau_1)), \tau_2) = 0,\\
&\tau_1 + \tau_2 + \tau_3 = 0.
\end{aligned}$$

Expanding about $\tau_1 = \tau_2 = 0$, we obtain

$$\begin{aligned}
&x_3 = x_0 + f^{(1)}(x_0)\tau_1 + f^{(s)}(x_0)\tau_2 + f^{(4)}(x_0)\tau_3 + O(2),\\
&H_2(x_0) + \mathcal{L}_{f^{(1)}} H_2(x_0)\tau_1 + O(2) = 0,\\
&H_1(x_0) + \mathcal{L}_{f^{(s)}} H_1(x_0)\tau_2 + \mathcal{L}_{f^{(1)}} H_1(x_0)\tau_1 + O(2) = 0,\\
&\tau_3 = -\tau_1 - \tau_2.
\end{aligned}$$

Hence,

$$x_3 = x_0 + (f^{(4)} - f^{(1)})\frac{H_2}{\mathcal{L}_{f^{(1)}} H_2} + (f^{(s)} - f^{(4)})\frac{H_2\mathcal{L}_{f^{(1)}} H_1 - H_1\mathcal{L}_{f^{(1)}} H_2}{\mathcal{L}_{f^{(s)}} H_1 \mathcal{L}_{f^{(1)}} H_2}.$$

A.3. Case II, PDM, $H_2(x_0) > 0$

We have,

$$x_2 = \Phi_3(\Phi_4(x_0, \tau_1), \tau_2),$$
$$H_2(x_1) = H_2(\Phi_4(x_0, \tau_1)) = 0,$$
$$H_1(x_2) = H_1(\Phi_3(\Phi_4(x_0, \tau_1)), \tau_2) = 0.$$

Expanding about $\tau_1 = 0$, we obtain

$$x_2 = x_0 + f^{(4)}(x_0)\tau_1 + f^{(3)}(x_0)\tau_2 + O(2),$$
$$H_2(x_0) + \mathcal{L}_{f^{(4)}} H_2(x_0)\tau_1 + O(2) = 0,$$
$$H_1(x_0) + \mathcal{L}_{f^{(4)}} H_1(x_0)\tau_1 + \mathcal{L}_{f^{(3)}} H_1(x_0)\tau_2 + O(2) = 0,$$

with $H_1(x_0) = 0$. Hence,

$$x_2 = x_0 - f^{(4)} \frac{H_2}{\mathcal{L}_{f^{(4)}} H_2} - f^{(3)} \frac{\mathcal{L}_{f^{(4)}} H_1}{\mathcal{L}_{f^{(s)}} H_1} \frac{H_2}{\mathcal{L}_{f^{(4)}} H_2}.$$

A.4. Case II, ZDM, $H_2(x_\Sigma) > 0$

We have,

$$x_2 = \Phi_4(\Phi_1(x_0, \tau_1), \tau_2),$$
$$H_2(x_1) = H_2(\Phi_1(x_0, \tau_1)) = 0,$$
$$\tau_1 + \tau_2 = 0.$$

Expanding about $\tau_1 = 0$, we obtain

$$x_2 = x_0 + f^{(1)}(x_0)\tau_1 + f^{(4)}(x_0)\tau_2 + O(2),$$
$$H_2(x_0) + \mathcal{L}_{f^{(1)}} H_2(x_0)\tau_1 + O(2) = 0,$$
$$\tau_2 = -\tau_1.$$

Hence,

$$x_2 = x_0 + (f^{(4)} - f^{(1)}) \frac{H_2}{\mathcal{L}_{f^{(1)}} H_2}.$$

References

[1] A.F. Filippov, Differential equations with discontinuous right-hand side, in: American Mathematical Society Translations Series, vol. 2, American Mathematical Society, 1964, pp. 199–231.
[2] A.F. Filippov, Differential Equations with Discontinuous Righthand Sides, Kluwer Academic Publishers, Dordrecht, 1988.
[3] Yu.A Kuznetsov, S. Rinaldi, A. Gragnani, One parameter bifurcations in planar Filippov systems, Internat. J. Bifur. Chaos 13 (2003) 2157–2188.
[4] Z.T. Zhusubaliyev, E. Mosekilde, Bifurcations and Chaos in Piecewise-Smooth Dynamical Systems, World Scientific, 2003.
[5] M. di Bernardo, C.J. Budd, A.R. Champneys, P. Kowalczyk, Piecewise-smooth Dynamical Systems: Theory and Applications, Springer-Verlag, 2008.
[6] A.B. Nordmark, Non-periodic motion caused by grazing incidence in an impact oscillator, J. Sound Vibration 145 (1991) 279–297.
[7] J. de Weger, D. Binks, J. Molenaar, W. van de Water, Generic behavior of grazing impact oscillators, Phys. Rev. Lett. 76 (1996) 3951–3954.
[8] M. di Bernardo, P. Kowalczyk, A. Nordmark, Sliding bifurcations: A novel mechanism for the sudden onset of chaos in dry-friction oscillators, Internat. J. Bifur. Chaos 13 (2003) 2935–2948.
[9] F. Angulo, E. Fossas, G. Olivar, Transition from periodicity to chaos in a pwm-controlled buck converter with ZAD strategy, Internat. J. Bifur. Chaos 15 (10) (2005) 3245–3264.
[10] M.I. Feigin, Doubling of the oscillation period with C-bifurcations in piecewise continouous systems, PMM J. Appl. Math. Mech. 34 (1970) 861–869.
[11] M.I. Feigin, On the generation of sets of subharmonic modes in a piecewise continuous system, PMM J. Appl. Math. Mech. 38 (1974) 810–818.
[12] M.I. Feigin, On the structure of C-bifurcation boundaries of piecewise continuous systems, PMM J. Appl. Math. Mech. 42 (1978) 820–829.
[13] H.E. Nusse, E. Ott, J.A. Yorke, Border-collision bifurcations: An explanation for observed bifurcation phenomena, Phys. Rev. E 49 (1994) 1073–1076.
[14] H.E. Nusse, J.A. Yorke, Border-collision bifurcations for piecewise smooth one-dimensional maps, Internat. J. Bifur. Chaos 5 (1995) 189–207.
[15] M. di Bernardo, M.I. Feigin, S.J. Hogan, M.E. Homer, Local analysis of C-bifurcations in n-dimensional piecewise smooth dynamical systems, Chaos, Solitons Fractals 10 (1999) 1881–1908.
[16] M. di Bernardo, C.J. Budd, A.R. Champneys, Corner collision implies border-collision bifurcation, Physica D 154 (2001) 171–194.
[17] M.di Bernardo, C.J. Budd, A.R. Champneys, Normal form maps for grazing bifurcations in n-dimensional piecewise-smooth dynamical systems, Physica D 160 (2001) 222–254.

[18] M. di Bernardo, P. Kowalczyk, A. Nordmark, Bifurcations of dynamical systems with sliding: Derivation of normal-form mappings, Physica D 170 (2002) 175–205.
[19] R.I. Leine, Bifurcations of equilibria in non-smooth continuous systems, Physica D 223 (2006) 121–137.
[20] P. Kowalczyk, M. di Bernardo, A.R. Champneys, S.J. Hogan, M. Homer, P.T. Piironinen, Two-parameter discontinuity-induced bifurcations of limit cycles: Classification and open problems, Internat. J. Bifur. Chaos 16 (3) (2006) 601–629.
[21] K. Popp, P. Shelter, Stick-slip vibrations and chaos, Philos. Trans. R. Soc. A 332 (1624) (1990) 89–105.
[22] M. di Bernardo, A.R. Champneys, C.J. Budd, Grazing, skipping and sliding: Analysis of the nonsmooth dynamics of the DC/DC buck converter, Nonlinearity 11 (1998) 858–890.
[23] J.Y. Hung, W.B. Gao, J.C. Hung, Variable structure control - a survey, IEEE Trans. Ind. Electron. 40 (1) (1993) 2–22.
[24] J.P. Aubin, A. Cellina, Differential Inclusions, Springer-Verlag, Berlin, 1984.
[25] P. Kowalczyk, Robust chaos and border-collision bifurcations in non-invertible piecewise-linear maps, Nonlinearity 18 (2005) 485–504.
[26] A.E. Aroudi, L. Benadero, E. Toribio, S. Machiche, Quasiperiodicity and chaos in the DC-DC buck-boost converter, Internat. J. Bifur. Chaos 10 (2) (2000) 359–371.
[27] L. Benadero, A.E. Aroudi, G. Olivar, E. Toribio, E. Gomez, Two-dimensional bifurcation diagrams. background pattern of fundamental dc-dc converters with pwm control, Internat. J. Bifur. Chaos 13 (2) (2003) 427–451.
[28] M. di Bernardo, C.J. Budd, A.R. Champneys, Grazing and border-collision in piecewise-smooth systems: A unified analytical framework, Phys. Rev. Lett. 86 (2001) 2553–2556.
[29] M.A. Aizerman, F.R. Gantmakher, On the stability of periodic motions, J. Appl. Math. Mech. (1958) 1065–1078.